Identification of optimal conditions for betatron x-ray generation in subcritical density plasma

Abdughupur. Ablimit, L. Q. Han,* X. Y. Zhao, C. OuYang, H. Wen,† and J. Q. Yu‡

Hunan Provincial Key Laboratory of High-Energy Scale Physics and Applications, School of Physics and Electronics, Hunan University, Changsha, 410082, China

(Received 23 May 2025; accepted 18 November 2025; published 13 January 2026)

Laser wakefield acceleration (LWFA) has enabled generation of high-energy electron beams and radiation sources, which are of great importance in high-energy density physics. However, identifying the optimal laser-plasma parameters—particularly variations in laser pulse duration and focal spot size—is crucial for producing not only high-charge, high-energy electron beams but also high-brightness, high-flux betatron radiation. In this study, we investigated the optimum laser parameters for generating high-charge electron beams and betatron radiation in subcritical density plasmas (SCDP). Three-dimensional particle-in-cell (3D-PIC) simulations show that a 550 TW laser pulse can generate electron beams with charges of several tens of nanocoulombs (nC) and energies up to 500 MeV. Furthermore, these electron beams produce high-brightness x-ray radiation, achieving a peak brightness of 1.6×10^{22} photons/(s mm^2 mrad^2 0.1% BW) at 10 keV, with a total photon number reaching 4×10^{12} (energy >1 keV).

DOI: 10.1103/gnck-rndz

I. INTRODUCTION

Laser wakefield acceleration (LWFA), first proposed by Tajima and Dawson [1], has emerged as a promising technology for compact, high-gradient particle acceleration and radiation generation. LWFA can achieve acceleration gradients up to 100 GV/m—3 orders of magnitude higher than those of conventional radio-frequency (rf) accelerators [2]—allowing for significant reduction in the size of particle accelerators and radiation sources. When an intense laser pulse ($a_0 \gg 1$) interacts with underdense plasma, the plasma electrons are expelled by the ponderomotive force of the laser, forming an ion cavity—commonly known as the bubble regime [3–6]. In this regime, the generation of high-energy monoenergetic electron beams with energies ranging from hundreds of MeV to multi-GeV has been demonstrated in both experiments and simulations [7–16]. Recent studies have demonstrated the potential of LWFA for producing x-rays through mechanisms such as betatron radiation [17–19], bright γ-rays generation using two-stage LWFA [20], Thomson (or Compton) scattering [21–24], x-ray free electron lasers (x-FELs) [25–27], and terahertz (THz) radiation [28]. These advances establish LWFA as a compelling alternative to rf accelerator-based radiation sources.

In LWFA, electrons injected into the plasma bubble are accelerated by a strong longitudinal electric field while undergoing transverse oscillations due to the focusing fields within the ion cavity [17–19]. These oscillations occur at the betatron frequency $\omega_\beta = \omega_p/\sqrt{2\gamma}$, resulting in the production of betatron radiation. Here, γ represents the Lorentz factor, and $\omega_p = \sqrt{4\pi n_p e^2/m_e}$ is the plasma frequency, where n_p is the plasma density, e is the electron charge, and m_e the electron mass. Betatron radiation provides a compact x-rays source characterized by femtosecond pulse duration, low divergence, and high brightness [29]. These features make it highly suitable for high-resolution x-ray imaging, time-resolved spectroscopy, ultrafast process studies, shock wave research, as well as applications in medical, warm dense matter, and biological fields [30–38].

The charge of the electron beam plays a crucial role in the generation of high-brilliance photon-flux beams. Various schemes have been proposed to generate high-charge electron beams, such as laser-solid interactions [39,40] and direct laser acceleration (DLA) [16,41–43]. However, these approaches typically result in electron beams characterized by broad energy spectra, lower peak energies, and large divergence angles. In LWFA, numerous research groups have explored methods to obtain high-charge electron beam [13,44]. Nevertheless, due to the beam-loading effect [45,46], the charge of the accelerated electron beam is generally limited to tens to hundreds of

*These authors contributed equally to this work.
†Contact author: hwen@hnu.edu.cn
‡Contact author: jinqing.yu@hnu.edu.cn

Published by the American Physical Society under the terms of the Creative Commons Attribution 4.0 International license. Further distribution of this work must maintain attribution to the author(s) and the published article's title, journal citation, and DOI.

pC. As a result, the photon number is restricted to approximately 10^7–10^8, and the laser-to-photon conversion efficiency remains relatively low at about 10^{-5} [29]. To overcome the beam-loading effect, Refs. [47,48] used subcritical density plasma (SCDP) to achieve a high-charge electron bunch and high-energy, high-flux betatron radiation. However, the shape of the bubble significantly affects its stability during propagation in plasma, thereby influencing the quality of electrons and radiation. Since the bubble shape is determined by the laser pulse duration and focal spot size. Therefore, identifying the optimal laser parameters is essential for producing stable, high-charge electron beams and high-brightness, high-flux radiation sources.

In this work, we present a numerical investigation of the optimal laser parameters for the injection, acceleration, and betatron radiation of highly relativistic electron bunches in LWFA using SCDP. We focus on the impact of laser pulse duration and focal spot size on the properties of electron beams and betatron radiation. Our 3D-PIC simulations demonstrate that a 550 TW femtosecond laser interacting with SCDP can efficiently accelerate electrons to energies exceeding 500 MeV, producing a high-charge beam of approximately 44 nC (for electrons with energy > 10 MeV). We confirm that the radiating electrons are primarily accelerated by the longitudinal electric field. Furthermore, highly brilliant betatron x-rays characterized by about 1.6×10^{22} photons/(s mm^2 mrad^2 0.1% BW) at 10 keV and a photon flux up to 4×10^{12} can be generated. Importantly, we demonstrate that under SCDP conditions, with a laser pulse duration of 12 T_0 and a focal spot size of 7 μm, the resulting radiation source achieves superior brightness, x-ray conversion efficiency, and photon yield compared with previous studies.

II. DETERMINING OPTIMAL PARAMETERS AND SIMULATION SETUP

The numerical simulations were conducted using the fully relativistic, open-source code EPOCH [49], which is widely used to study electron acceleration and radiation properties. In the 3D simulation, linearly polarized Gaussian laser pulses with a wavelength of $\lambda = 0.8$ μm, a laser pulse duration of 12 T_0, and a focal spot size of 7 μm were employed. The normalized amplitude was $a_0 = \frac{eE_0}{m_e c \omega_L} = 20$, corresponding to an intensity of 8.6×10^{20} W/cm^2, where E_0 is the laser electric field amplitude. The laser had a Gaussian spatial profile and a sin^2 temporal profile. The pulses were focused at the left boundary of the plasma target (at $x = 0$) and propagated along the positive x direction, with a fixed duration of 1.45 ps. A moving-window technique was employed, with the window propagating at the speed of light c. The simulation domain had a box size of $50 \times 28 \times 28$ μm along the x, y, and z directions and a grid resolution of $800 \times 280 \times 280$ cells. The x axis was aligned with the laser propagation direction, while the y axis corresponded to the laser polarization direction. The plasma target consisted of a fully ionized, uniform mixture of electrons, H^+ ions, and C^{6+} ions with respective densities of 0.1 n_c, 0.01 n_c, and 0.015 n_c, where n_c is the critical density, defined as $n_c = \frac{m_e \epsilon_0 \omega_L^2}{e^2}$, ϵ_0 is the vacuum permittivity, ω_L is the laser frequency, and n_c has a corresponding value of 1.74×10^{21} cm^{-3}. Each simulation cell contained 16, 6, and 6 particles for electrons, H^+ ions, and C^{6+} ions, respectively.

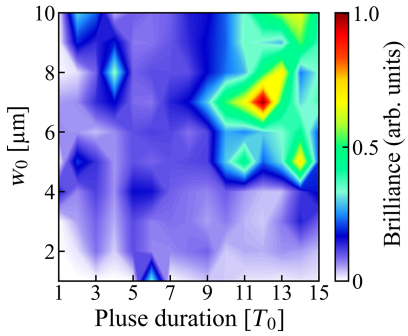

FIG. 1. Variation in betatron radiation brightness with respect to the laser pulse duration and focal spot size (w_0) is presented in a 2D simulation. Color bar represents photon brightness at 10 keV.

For the two-dimensional (2D) simulations, we adopted the same parameters as in the 3D case. In 2D simulations, we investigated the brightness of laser-driven betatron radiation from uniform plasmas by varying the laser pulse duration (1 T_0 to 15 T_0, where T_0 represents the laser cycle period) and the focal spot radius (1 and 10 μm), as shown in Fig. 1. In 2D parameter scans, we identified the optimal laser parameters for generating high-brightness betatron radiation laser duration of 12 T_0 and laser focal spot size of 7 μm. Beyond this optimal balance, increasing either the laser duration or focal spot size leads to reduced radiation brightness due to instability in the bubble structure and increased electron beam divergence. The detailed relationship between laser parameters and radiation brightness is illustrated in Fig. 1 and further discussed through an examination of the electron beam properties and betatron radiation. In addition, the 550 TW, femtosecond-class laser pulse used in our simulations is consistent with the capabilities of existing high-power laser facilities, such as SILEX-II [50], ELI-NP [51], PHELIX [52], and SULF [53], which routinely deliver multihundred-terawatt to petawatt pulses with comparable durations and focal spot sizes. This confirms that the laser-plasma interaction regime investigated in this work is experimentally accessible with present-day technology.

III. ELECTRON ACCELERATION AND BETATRON RADIATION

To investigate the acceleration of high-energy electrons inside the bubble and the properties of the resulting

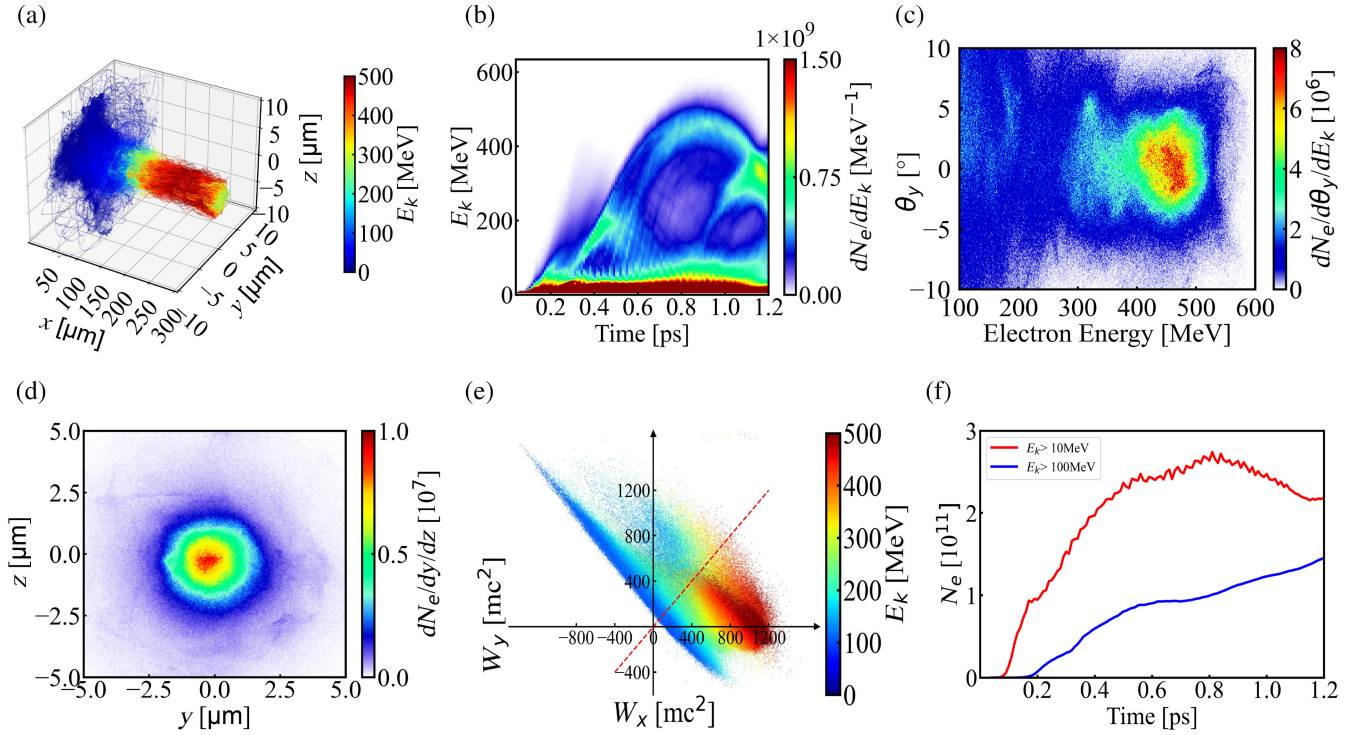

FIG. 2. (a) 3D-PIC simulation of electron trajectories. (b) Energy distribution function of all electrons as a function of time. (c) Angular energy distribution of the accelerated electrons at 900 fs, where θ is defined as $\theta = \arctan(p_y/p_x)$. (d) Spatial distribution of the electrons at 1100 fs, with color representing beam density. (e) Time-integrated work performed on energy-gain plane (W_x, W_y) of electrons with the energy distribution across the transverse (W_y) and longitudinal (W_x) directions at $t = 900$ fs. (f) Red line depicts the evolution of the total number of high-energy electrons with energies exceeding 10 MeV, while the blue line represents those with energies exceeding 100 MeV.

betatron radiation, we analyzed more than 3700 randomly selected electron trajectories ($E_k > 100$ MeV) in Fig. 2(a). The color of each line represents the energy of the macroparticle. The laser expels electrons via relativistic self-focusing, forming a bubble structure, where electrons are primarily accelerated by the wakefield, achieving energy gains exceeding 500 MeV over distances longer than 200 μm. The strong transverse oscillations of these high-energy electrons in the bubble regime can efficiently radiate a large number of x-ray photons, known as betatron radiation. Figure 2(b) shows the evolution of the electron energy spectrum over 1.2 ps, indicating that most electrons achieve higher energies. Figure 2(c) depicts the spectral-angular distribution of the electron bunch, revealing a divergence angle of approximately $\theta_y \approx 6°$ in the polarized direction at 900 fs. This divergence is larger than that typically observed in standard LWFA but smaller than in DLA [2,42,54]. Figure 2(d) illustrates the transverse size distribution of the electrons, which is well centered on the transverse bunch size of 4×4 μm (FWHM) at 1.1 ps. Figure 2(e) shows the contributions of LWFA and DLA [54–56] to the energy gain of high-energy electrons. The total energy gain of each electron is divided into two components: $W = W_x + W_y$, where W_x represents the energy gain from the longitudinal field and W_y corresponds to the energy gain from the transverse field. Specifically, these components are defined as $W_x = -\int_0^t e\mathbf{E}_x v_x/m_e c^2\, dt$ and $W_y = -\int_0^t e\mathbf{E}_y v_y/m_e c^2\, dt$, where v_x and v_y are electron longitudinal and transverse velocities, respectively [54]. The dominant longitudinal electric field primarily accelerates electrons through the LWFA mechanism, as described by W_x. The transverse electric field contributes to the electron energy gain through the DLA mechanism, mediated by $\vec{v} \times \vec{B}$ forces. As the bubble forms, LWFA dominates the generation of relativistic electrons, with $W_x > W_y$. The electrons gain energy primarily from the longitudinal electric field, with W_x reaching up to 600 MeV, while the transverse energy gain from both the laser and channel fields is limited to below 100 MeV. This demonstrates that LWFA is the dominant acceleration mechanism for high-energy electrons, with the DLA contribution being negligible. This observation is consistent with the oscillatory behavior of high-energy electrons shown in the trajectory trace Fig. 2(a). Moreover, the substantial forward acceleration of electrons, combined with their betatron oscillations within the bubble region, highlights the potential of this process as an efficient x-rays source. This is particularly evident at each turning point of the oscillations. Figure 2(f) illustrated the temporal evolution of the electron count (N_e) for particles with energies above 10 and 100 MeV, represented by two separate curves (red and blue). The data

show that approximately 2.75×10^{11} electrons have energies above 10 MeV, while around 1.5×10^{11} electrons have energies above 100 MeV. The accelerated electron bunches carry total charges of up to 44 nC for electrons with energies above 10 MeV and 23 nC for energies above 100 MeV, with laser energy conversion efficiencies of 43.7% and 39.8%, respectively. These results are higher than those of the previous report [57,58]. Thus, a high-charge electron bunch provides a promising source for bright betatron radiation. Leveraging this high-charge, high-energy electron beam, we further investigate the potential for high-flux, high-brightness x-ray generation through interactions between relativistic femtosecond lasers and extended SCDP.

In the bubble regime, the plasma structure also acts as a wiggler, causing relativistic electrons to undergo forward and transverse oscillations, emitting betatron radiation, as shown in Fig. 3. The oscillatory motion of the electrons in this regime can be described by the following Liénard-Wiechert potential [59]:

$$\frac{d^2I}{d\Omega d\omega} = \frac{e^2}{16\pi^3\epsilon_0 c}\left|\int_{-\infty}^{\infty}\frac{\{\mathbf{n}\times[(\mathbf{n}-\boldsymbol{\beta})\times\dot{\boldsymbol{\beta}}]\}e^{i\omega\{t-\mathbf{n}\cdot\mathbf{r}(t)/c\}}}{(1-\boldsymbol{\beta}\cdot\mathbf{n})^2}dt\right|^2, \tag{1}$$

where $\mathbf{r}(t)$ represents the electron's trajectory, $\boldsymbol{\beta}$ denotes the normalized velocity, and $\mathbf{n}$ is the unit vector, respectively.

The transverse acceleration produces synchrotronlike radiation, which is emitted in a narrow forward-directed cone. The betatron radiation spectrum resembles that of the wiggler regime characterized by the betatron oscillation strength parameter K, defined as $K = 1.33 \times 10^{-10}\sqrt{\gamma n_e\,(\mathrm{cm}^{-3})}\,r_\beta(\mu\mathrm{m})$, where r_β is the betatron amplitude and c represents the speed of light. Under typical LWFA conditions, where $K \gg 1$, the number of photons emitted per electron per oscillation period scales approximately as $N_{\mathrm{ph}} \propto K$. Furthermore, N_{ph} can be significantly increased by employing an electron beam with higher charge and increasing the number of oscillations within the plasma wakefield. The mean number of photons emitted by the electron beam in the plasma wiggler is given by [18]:

$$\langle N_{\mathrm{ph}}\rangle \approx \frac{2\pi}{9}\frac{e^2}{hc}N_\beta N_e K \approx 5.6\times 10^{-3} N_\beta N_e K, \tag{2}$$

where N_β represents the number of betatron oscillation periods, and N_e represents the number of wiggling electrons, respectively. In accordance with Eq. (2), the betatron x-rays radiation is estimated to be approximately $N_{\mathrm{ph}} \propto 10^{12}$, which agrees reasonably well with the simulation results.

Figure 3(a) shows the temporal evolution of the photon number. The total number of photons with energy > 1 keV exceeds 4×10^{12}, which is higher than the previous result [60], indicating a remarkable increase in photon production,

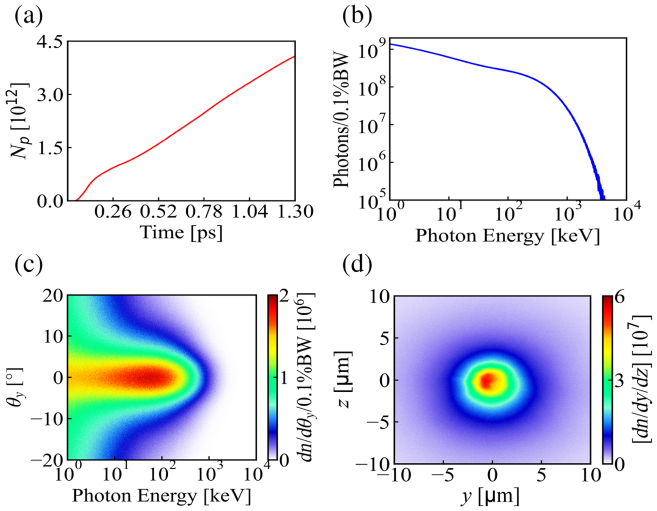

FIG. 3. Results of a 3D-PIC simulation: (a) time evolution of photon number (N_p) at energy > 1 keV. (b) Energy spectra of the betatron radiation per 0.1% bandwidth (BW) at 1.1 ps. (c) Angular distribution of the betatron radiation at 1.1 ps. (d) Transverse distribution of the x-ray photons at 1.1 ps.

corresponding to a laser-to-photon energy conversion efficiency of 1.9×10^{-2}%, which is one order of magnitude higher than in other betatron radiation results [61–63]. The obtained photon energy spectrum at 1.1 ps is shown in Fig. 3(b). The simulation calculates and describes the distribution of all emitted photons within the simulation region, revealing that the photon spectrum exhibits synchrotronlike characteristics of a value of $K \gg 1$, which are determined by the synchrotron function $S(\omega/\omega_c)$, $S(x) = x\int_x^\infty K_{5/3}(\xi)d\xi$, where $K_{5/3}$ is a modified Bessel function of the second kind [59], $x = \omega/\omega_c$, ω_c is a critical frequency. The source up to about 10^9 photons/0.1% bandwidth (BW).

Figure 3(c) shows the angular distribution of the photon energy presented, revealing a divergence angle of approximately 6.5° (FWHM). The peak brightness of betatron x-rays is calculated at 10 keV, with the peak brilliance reaching to 1.6×10^{22} photons/(s mm^2 mrad^2 0.1% BW). This value is an order of magnitude higher than previously reported values [38,63,64] and is comparable to that achieved by third-generation synchrotron radiation sources. Figure 3(d) further illustrated the transverse plane (y, z) distribution of the photons, showing a highly compact radiation source with a bunch size of 2.5×2.5 μm.

As the laser pulse propagates in the SCDP, the ponderomotive force expels the electrons, creating an ion cavity, and self-injection occurs. Figure 4 further analyzes the transverse size of the electron beam under different laser parameters. Figure 4(a) shows the electron injection and acceleration process when the laser pulse duration is 12 T_0 and the focal spot size is 7 μm, with the electron beam energy reaching several hundred MeV and the laser field strength being 3 TV/m, efficiently transferring energy to the electrons. The electron density map confirms strong

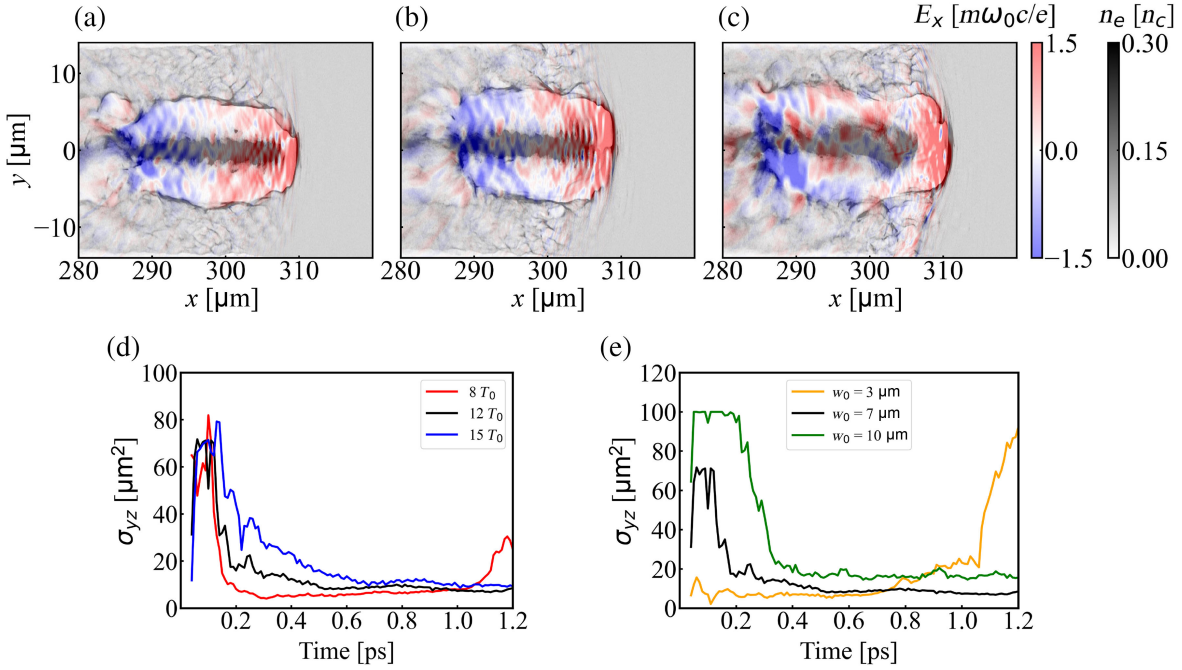

FIG. 4. 3D-PIC simulation of electron self-injection evolution in a plasma bubble at 1100 fs with different laser parameters. (a) Laser duration of 12 T_0 and focal spot size of 7 μm. (b) Laser duration of 15 T_0 and focal spot size of 7 μm. (c) Laser duration of 12 T_0 and focal spot size of 10 μm. Color maps represent E_x longitudinal electric field and n_e electron number density. (d) Evolution of the electron beam transverse size over time for a fixed laser focal spot size of 7 μm, with pulse durations of 8 T_0, 12 T_0, and 15 T_0. (e) Evolution of the electron beam transverse size over time for a fixed laser duration of 12 T_0, with focal spot size of 3, 7, and 10 μm.

energy coupling, while the relatively high plasma density ensures the generation of a high-charge beam. In this regime, self-modulation leads to transverse energy redistribution [65], and near-elliptical light-filled cavities ("laser bullets") are formed, characteristic of the transition to the self-trapping (RST) regime [66]. Figures 4(b) and 4(c) show the relativistic self-focusing occurs with continuous longitudinal expansion of the bubble and sustained continuous self-injection. Although self-focusing effects induce massive electron bunches and continuous self-injection, laser hosing instability [63,67] can result in the generation of uncontrollable electron beams and radiation sources, leading to an increased transverse beam size. These processes gradually transform the initially stable bubble into an unstable structure, accompanied by increased oscillations and beam divergence. This result is consistent with Figs. 4(d) and 4(e). Figure 4(d) illustrates the temporal evolution of the transverse size σ_{yz} of the electron beam up to 1.1 ps. The transverse size σ_{yz} rapidly increases to a peak at the early stage, then gradually decreases and eventually stabilizes. For a laser pulse duration of 12 T_0 (dark line), the beam reaches the smallest and most stable transverse size of about 4 × 4 μm, indicating the best transverse focusing performance. For a duration of 8 T_0 (red line), the transverse size exhibits a higher peak and slower stabilization; however, at 1.1 ps, the size suddenly increases. By increasing the laser pulse duration, the acceleration regime transitions from LWFA to SMLWFA [68]. For a 15 T_0 pulse (blue line), the transverse beam size remains larger than that of the 12 T_0 case, reflecting beam instabilities induced by this transition. As a result, the x-ray brilliance is reduced due to the increased beam divergence and the longer pulse duration compared to the LWFA regime. Figure 4(e) shows the temporal evolution of the transverse size σ_{yz} of the electron beam under different laser focal spot sizes with a fixed laser pulse duration. For the small laser focal spot (orange line), the transverse size of the electron beam is initially the smallest within the first 800 fs. However, it suddenly increases after ($t > 800$ fs) because the lower laser energy in the small spot case is more easily dissipated. This dissipation triggers the release of transverse energy, which destabilizes the bubble and leads to a rapid growth of the size of the transverse beam, ultimately resulting in an unstable bubble evolution [66]. For the large laser focal spot (green line), continuous injection of electrons occurs throughout the laser evolution. This leads to the formation of a high-density region at approximately 1.1 ps as accelerated electrons overtake the plasma front. The electric field of this region perturbs the bubble's potential, ultimately destabilizing its structure. Furthermore, this disruption is accompanied by a significant laser hosing instability, which increases the electron beam divergence and results in a larger transverse beam size of approximately 5 × 5 μm. Under the optimal laser parameters (black line), the electron beam maintains a more stable transverse size, enabling the

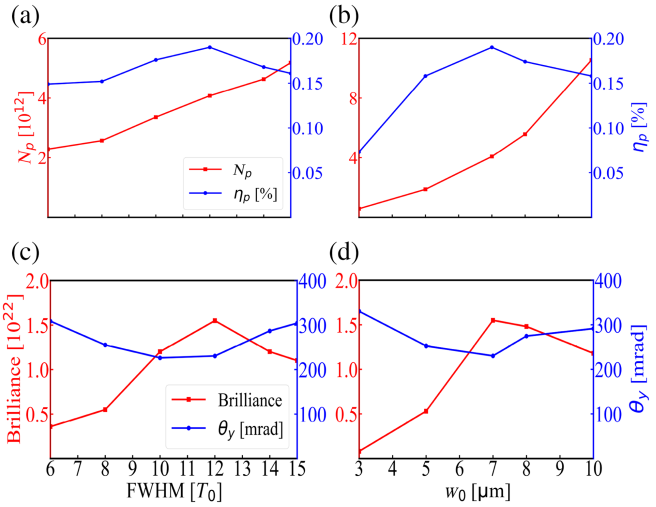

FIG. 5. Results from 3D-PIC simulations on the effects of laser duration and focal spot size on radiation properties. (a) and (c) show fixed focal spot size of 7 μm, varying laser duration: the total number of photons N_p and laser-to-photon conversion efficiency η_p. (b) and (d) show fixed laser duration of 12 T_0, varying laser focal spot size: the peak brilliance and divergence angle θ_y.

generation of high-charge electron beams and high-brightness betatron radiation sources.

Figure 5 presents the results of betatron radiation under different laser parameters. Figures 5(a) and 5(c) show the effects of laser duration ranging from 6 T_0 to 15 T_0 with a fixed spot size of 7 μm. The photon number N_p and the conversion efficiency η_p are plotted as functions of the laser duration. The number of photons increases nearly linearly with T_0, rising from approximately 2×10^{12} at 6 T_0 to 5.5×10^{12} at 15 T_0. This is because longer laser durations facilitate the triggering of betatron radiation. The conversion efficiency η_p for photons with energy exceeding 1 keV also increases with T_0, reaching a maximum of 0.19% at 12 T_0. However, further increases in laser duration do not always improve performance, as η_p slowly decreases at larger durations. Photon brilliance exhibits a similar trend, peaking at approximately 1.6×10^{22} photons/(s mm^2 mrad^2 0.1% BW) at 12 T_0 for photon energies of 10 keV. Beyond 12 T_0, the brilliance decreases (red line), which can be attributed to the increased angular divergence of betatron radiation, as shown in Figs. 5(c) and 5(d). This divergence arises from the transition of the acceleration regime from LWFA to SMLWFA, which enhances hosing instability.

Figures 5(b) and 5(d) illustrate the effect of varying the laser focal spot size from 3 to 10 μm, with a fixed laser duration of 12 T_0. The photon number N_p increases rapidly with the focal spot size, reaching 11.5×10^{12} at a spot size of 10 μm. The conversion efficiency η_p for photons with energies exceeding 1 keV also grows with T_0, reaching a maximum of 0.19% at 12 T_0. A small focal spot size is disadvantageous because it increases the electron beam divergence [69], resulting in lower brilliance (red line). The angular divergence θ_y (blue line) decreases from 350 mrad at a focal spot size of 3 μm to 250 mrad at 7 μm, indicating a reduction in photon beam divergence. These results, shown in Fig. 5(b), are consistent with the findings in Figs. 4(d) and 4(e).

IV. CONCLUSION

In this study, we conducted full-scale 3D-PIC simulations to investigate the optimal parameters for generating high-charge, high-energy electron beams and high-brightness, high-photon-flux betatron radiation in SCDP channels. Under optimal parameters, with a laser duration of 12 T_0 and a focal spot size of 7 μm, we achieved total electron bunch charge of approximately 44 nC ($E_k > 10$ MeV), an energy of more than 500 MeV, and a laser-to-electron conversion efficiency of 43.7%, which is nearly twice as high as the 23% reported in Ref. [58]. The betatron radiation reached photon energies exceeding 1 keV, with a photon number of approximately 4×10^{12}, a peak brightness of 1.6×10^{22} photons/(s mm^2 mrad^2 0.1%BW) at 10 keV, and a divergence angle of 6.5°. The maximum laser-to-photon conversion efficiency was 0.19%. Our findings also reveal that increasing the laser duration or focal spot size leads to higher electron energy and photon number. However, larger pulse durations or spot sizes result in reduced brilliance due to increased electron beam divergence. Our study has made significant progress by identifying the optimal laser parameters, successfully generating stable, high-charge electron beams, and high-brightness, high-flux betatron radiation. Specifically, a brilliance of order 10^{22} photons/(s mm^2 mrad^2 0.1%BW) pulsed synchrotron x-rays from plasma wakes are well suited for high-resolution phase-contrast imaging [70]. High-energy electrons and high-charge electron beams are key to the generation of x-ray sources [71].

ACKNOWLEDGMENTS

This work was supported by the Natural Science Foundation of China (Grants No. 12175058 and No. 11921006), National Science Fund of Hunan Province for Distinguished Young Scholars No. 2024JJ2009.

DATA AVAILABILITY

The data that support the findings of this article are not publicly available upon publication because it is not technically feasible and/or the cost of preparing, depositing, and hosting the data would be prohibitive within the terms of this research project. The data are available from the authors upon reasonable request.

[1] T. Tajima and J. M. Dawson, Laser electron accelerator, Phys. Rev. Lett. **43**, 267 (1979).

[2] E. Esarey, C. B. Schroeder, and W. P. Leemans, Physics of laser-driven plasma-based electron accelerators, Rev. Mod. Phys. **81**, 1229 (2009).

[3] W. Lu, M. Tzoufras, C. Joshi, F. S. Tsung, W. B. Mori, J. Vieira, R. A. Fonseca, and L. O. Silva, Generating multi-GeV electron bunches using single stage laser wakefield acceleration in a 3D nonlinear regime, Phys. Rev. ST Accel. Beams **10**, 061301 (2007).

[4] W. Lu, C. Huang, M. Zhou, W. B. Mori, and T. Katsouleas, Nonlinear theory for relativistic plasma wakefields in the blowout regime, Phys. Rev. Lett. **96**, 165002 (2006).

[5] A. Pukhov and J. M. ter Vehn, Laser wake field acceleration: The highly non-linear broken-wave regime, Appl. Phys. B **74**, 355 (2002).

[6] W. Lu, C. Huang, M. Zhou, M. Tzoufras, F. S. Tsung, W. B. Mori, and T. Katsouleas, A nonlinear theory for multidimensional relativistic plasma wave wakefields, Phys. Plasmas **13**, 056709 (2006).

[7] S. P. D. Mangles, C. D. Murphy, Z. Najmudin, A. G. R. Thomas, J. L. Collier, A. E. Dangor, E. J. Divall, P. S. Foster, J. G. Gallacher, and C. J. Hooker, Monoenergetic beams of relativistic electrons from intense laser-plasma interactions, Nature (London) **431**, 535 (2004).

[8] C. G. R. Geddes, C. Toth, J. Van Tilborg, E. Esarey, C. B. Schroeder, D. Bruhwiler, C. Nieter, J. Cary, and W. P. Leemans, High-quality electron beams from a laser wakefield accelerator using plasma-channel guiding, Nature (London) **431**, 538 (2004).

[9] J. Faure, Y. Glinec, A. Pukhov, S. Kiselev, S. Gordienko, E. Lefebvre, J. P. Rousseau, F. Burgy, and V. Malka, A laser–plasma accelerator producing monoenergetic electron beams, Nature (London) **431**, 541 (2004).

[10] A. J. Gonsalves *et al.*, Petawatt laser guiding and electron beam acceleration to 8 GeV in a laser-heated capillary discharge waveguide, Phys. Rev. Lett. **122**, 084801 (2019).

[11] C. Aniculaesei, T. Ha, S. Yoffe, L. Labun, S. Milton, E. McCary, M. M. Spinks, H. J. Quevedo, O. Z. Labun, R. Sain *et al.*, The acceleration of a high-charge electron bunch to 10 GeV in a 10-cm nanoparticle-assisted wakefield accelerator, Matter Radiat. Extremes **9**, 014001 (2024).

[12] A. Picksley, J. Stackhouse, C. Benedetti, K. Nakamura, H. Tsai, R. Li, B. Miao, J. Shrock, E. Rockafellow, H. Milchberg *et al.*, Matched guiding and controlled injection in dark-current-free, 10-GeV-class, channel-guided laser-plasma accelerators, Phys. Rev. Lett. **133**, 255001 (2024).

[13] L. Ke, K. Feng, W. Wang, Z. Qin, C. Yu, Y. Wu, Y. Chen, R. Qi, Z. Zhang, Y. Xu *et al.*, Near-GeV electron beams at a few per-mille level from a laser wakefield accelerator via density-tailored plasma, Phys. Rev. Lett. **126**, 214801 (2021).

[14] E. Brunetti, R. Shanks, G. Manahan, M. Islam, B. Ersfeld, M. Anania, S. Cipiccia, R. Issac, G. Raj, G. Vieux *et al.*, Low emittance, high brilliance relativistic electron beams from a laser-plasma accelerator, Phys. Rev. Lett. **105**, 215007 (2010).

[15] W. Wang, W. Li, J. Liu, Z. Zhang, R. Qi, C. Yu, J. Liu, M. Fang, Z. Qin, C. Wang *et al.*, High-brightness high-energy electron beams from a laser wakefield accelerator via energy chirp control, Phys. Rev. Lett. **117**, 124801 (2016).

[16] R. Babjak, L. Willingale, A. Arefiev, and M. Vranic, Direct laser acceleration in underdense plasmas with multi-pw lasers: A path to high-charge, GeV-class electron bunches, Phys. Rev. Lett. **132**, 125001 (2024).

[17] A. Rousse, K. T. Phuoc, R. Shah, A. Pukhov, E. Lefebvre, V. Malka, S. Kiselev, F. Burgy, J.-P. Rousseau, D. Umstadter *et al.*, Production of a keV x-ray beam from synchrotron radiation in relativistic laser-plasma interaction, Phys. Rev. Lett. **93**, 135005 (2004).

[18] S. Kiselev, A. Pukhov, and I. Kostyukov, X-ray generation in strongly nonlinear plasma waves, Phys. Rev. Lett. **93**, 135004 (2004).

[19] S. Cipiccia, M. R. Islam, B. Ersfeld, R. P. Shanks, E. Brunetti, G. Vieux, X. Yang, R. C. Issac, S. M. Wiggins, G. H. Welsh *et al.*, Gamma-rays from harmonically resonant betatron oscillations in a plasma wake, Nat. Phys. **7**, 867 (2011).

[20] X.-L. Zhu, M. Chen, S.-M. Weng, T.-P. Yu, W.-M. Wang, F. He, Z.-M. Sheng, P. McKenna, D. A. Jaroszynski, and J. Zhang, Extremely brilliant GeV γ-rays from a two-stage laser-plasma accelerator, Sci. Adv. **6**, eaaz7240 (2020).

[21] G. Sarri, D. J. Corvan, W. Schumaker, J. M. Cole, A. Di Piazza, H. Ahmed, C. Harvey, C. H. Keitel, K. Krushelnick, S. P. D. Mangles, Z. Najmudin, D. Symes, A. G. R. Thomas, M. Yeung, Z. Zhao, and M. Zepf, Ultrahigh brilliance multi-MeV γ-ray beams from non-linear relativistic Thomson scattering, Phys. Rev. Lett. **113**, 224801 (2014).

[22] K. Ta Phuoc, S. Corde, C. Thaury, V. Malka, A. Tafzi, J. P. Goddet, R. C. Shah, S. Sebban, and A. Rousse, All-optical Compton gamma-ray source, Nat. Photonics **6**, 308 (2012).

[23] S. Chen, N. Powers, I. Ghebregziabher, C. Maharjan, C. Liu, G. Golovin, S. Banerjee, J. Zhang, N. Cunningham, A. Moorti *et al.*, MeV-energy x rays from inverse Compton scattering with laser-wakefield accelerated electrons, Phys. Rev. Lett. **110**, 155003 (2013).

[24] M. Mirzaie, C. I. Hojbota, D. Y. Kim, V. B. Pathak, T. G. Pak, C. M. Kim, H. W. Lee, J. W. Yoon, S. K. Lee, Y. J. Rhee *et al.*, All-optical nonlinear Compton scattering performed with a multi-petawatt laser, Nat. Photonics **18**, 1212 (2024).

[25] M. Fuchs, R. Weingartner, A. Popp, Z. Major, S. Becker, J. Osterhoff, I. Cortrie, B. Zeitler, R. Hörlein, G. D. Tsakiris *et al.*, Laser-driven soft-x-ray undulator source, Nat. Phys. **5**, 826 (2009).

[26] A. Maier, A. Meseck, S. Reiche, C. Schroeder, T. Seggebrock, and F. Gruener, Demonstration scheme for a laser-plasma-driven free-electron laser, Phys. Rev. X **2**, 031019 (2012).

[27] W. Wang, K. Feng, L. Ke, C. Yu, Y. Xu, R. Qi, Y. Chen, Z. Qin, Z. Zhang, M. Fang *et al.*, Free-electron lasing at 27 nanometres based on a laser wakefield accelerator, Nature (London) **595**, 516 (2021).

[28] L. Wang, Z. Zhang, S. Chen, Y. Chen, X. Hu, M. Zhu, W. Yan, H. Xu, L. Sun, M. Chen *et al.*, Millijoule terahertz radiation from laser wakefields in nonuniform plasmas, Phys. Rev. Lett. **132**, 165002 (2024).

[29] S. Corde, K. Ta Phuoc, G. Lambert, R. Fitour, V. Malka, A. Rousse, A. Beck, and E. Lefebvre, Femtosecond x rays from laser-plasma accelerators, Rev. Mod. Phys. **85**, 1 (2013).

[30] F. Albert, N. Lemos, J. Shaw, P. King, B. Pollock, C. Goyon, W. Schumaker, A. Saunders, K. Marsh, A. Pak *et al.*, Betatron x-ray radiation in the self-modulated laser wakefield acceleration regime: Prospects for a novel probe at large scale laser facilities, Nucl. Fusion **59**, 032003 (2018).

[31] D. C. Swift, A. L. Kritcher, J. A. Hawreliak, A. Lazicki, and R. W. Falcone, Absolute Hugoniot measurements from a spherically convergent shock using x-ray radiography, Rev. Sci. Instrum. **89**, 053505 (2018).

[32] A. Ravasio, M. Koenig, S. Le Pape, A. Benuzzi-Mounaix, H. S. Park, C. Cecchetti, P. Patel, A. Schiavi, N. Ozaki, and A. Mackinnon, Hard x-ray radiography for density measurement in shock compressed matter, Phys. Plasmas **15**, 1178 (2008).

[33] J. C. Wood, D. J. Chapman, K. Poder, N. C. Lopes, M. E. Rutherford, T. G. White, F. Albert, K. T. Behm, N. Booth, and J. S. J. Bryant, Ultrafast imaging of laser driven shock waves using betatron x-rays from a laser wakefield accelerator, Sci. Rep. **8**, 11010 (2018).

[34] J. M. Cole, J. C. Wood, N. C. Lopes, K. Poder, R. L. Abel, S. Alatabi, J. S. J. Bryant, A. Jin, S. Kneip, and K. Mecseki, Laser-wakefield accelerators as hard x-ray sources for 3D medical imaging of human bone, Sci. Rep. **5**, 13244 (2015).

[35] A. Dpp, L. Hehn, J. Goetzfried, J. Wenz, and S. Karsch, Quick x-ray microtomography using a laser-driven betatron source, Optica **5**, 199 (2018).

[36] S. Kneip, C. Mcguffey, F. Dollar, M. S. Bloom, V. Chvykov, G. Kalintchenko, K. Krushelnick, A. Maksimchuk, S. P. D. Mangles, and T. Matsuoka, X-ray phase contrast imaging of biological specimens with femtosecond pulses of betatron radiation from a compact laser plasma wakefield accelerator, Appl. Phys. Lett. **99**, 093701 (2011).

[37] B. Mahieu, N. Jourdain, K. Ta Phuoc, F. Dorchies, J.-P. Goddet, A. Lifschitz, P. Renaudin, and L. Lecherbourg, Probing warm dense matter using femtosecond x-ray absorption spectroscopy with a laser-produced betatron source, Nat. Commun. **9**, 3276 (2018).

[38] O. N. Rosmej, X. Shen, A. Pukhov, L. Antonelli, F. Barbato, M. Gyrdymov, M. M. Günther, S. Zähter, V. S. Popov, N. G. Borisenko *et al.*, Bright betatron radiation from direct-laser-accelerated electrons at moderate relativistic laser intensity, Matter Radiat. Extremes **6**, 048401 (2021).

[39] T. Cowan, A. Hunt, T. Phillips, S. Wilks, M. Perry, C. Brown, W. Fountain, S. Hatchett, J. Johnson, M. Key *et al.*, Photonuclear fission from high energy electrons from ultraintense laser-solid interactions, Phys. Rev. Lett. **84**, 903 (2000).

[40] Y. Ma, J. Zhao, Y. Li, D. Li, L. Chen, J. Liu, S. J. Dann, Y. Ma, X. Yang, Z. Ge *et al.*, Ultrahigh-charge electron beams from laser-irradiated solid surface, Proc. Natl. Acad. Sci. U.S.A. **115**, 6980 (2018).

[41] A. Pukhov, Z.-M. Sheng, and J. Meyer-ter Vehn, Particle acceleration in relativistic laser channels, Phys. Plasmas **6**, 2847 (1999).

[42] T. W. Huang, A. P. L. Robinson, C. T. Zhou, B. Qiao, B. Liu, S. C. Ruan, X. T. He, and P. A. Norreys, Characteristics of betatron radiation from direct-laser-accelerated electrons, Phys. Rev. E **93**, 063203 (2016).

[43] A. E. Hussein, A. V. Arefiev, T. Batson, H. Chen, R. Craxton, A. S. Davies, D. H. Froula, Z. Gong, D. Haberberger, Y. Ma *et al.*, Towards the optimisation of direct laser acceleration, New J. Phys. **23**, 023031 (2021).

[44] A. Buck, J. Wenz, J. Xu, K. Khrennikov, K. Schmid, M. Heigoldt, J. M. Mikhailova, M. Geissler, B. Shen, F. Krausz *et al.*, Shock-front injector for high-quality laser-plasma acceleration, Phys. Rev. Lett. **110**, 185006 (2013).

[45] C. Rechatin, X. Davoine, A. Lifschitz, A. B. Ismail, J. Lim, E. Lefebvre, J. Faure, and V. Malka, Observation of beam loading in a laser-plasma accelerator, Phys. Rev. Lett. **103**, 194804 (2009).

[46] M. Tzoufras, W. Lu, F. S. Tsung, C. Huang, W. B. Mori, T. Katsouleas, J. Vieira, R. Fonseca, and L. O. Silva, Beam loading in the nonlinear regime of plasma-based acceleration, Phys. Rev. Lett. **101**, 145002 (2008).

[47] R. Huang, L. Han, Y. Shou, D. Wang, T. Yu, J. Yu, and X. Yan, High-flux and bright betatron x-ray source generated from femtosecond laser pulse interaction with sub-critical density plasma, Opt. Lett. **48**, 819 (2023).

[48] L. Han, J. Cai, Y. Shou, X. Liu, J. Yu, and X. Yan, Linear Breit-Wheeler process driven by compact lasers, Phys. Rev. E **108**, 055208 (2023).

[49] T. Arber, K. Bennett, C. Brady, A. Lawrence-Douglas, M. Ramsay, N. J. Sircombe, P. Gillies, R. Evans, H. Schmitz, A. Bell *et al.*, Contemporary particle-in-cell approach to laser-plasma modelling, Plasma Phys. Controlled Fusion **57**, 113001 (2015).

[50] K. Zhou, X. Huang, X. Zeng, N. Xie, Y. Zuo, Y. Guo, D. Jiang, W. Dai, Q. Xue, W. Huang *et al.*, Improvement of focusing performance for a multi-petawatt OPCPA laser facility, Laser Phys. **28**, 125301 (2018).

[51] K. Tanaka, K. Spohr, D. Balabanski, S. Balascuta, L. Capponi, M. Cernaianu, M. Cuciuc, A. Cucoanes, I. Dancus, A. Dhal *et al.*, Current status and highlights of the ELI-NP research program, Matter Radiat. Extremes **5**, 024402 (2020).

[52] V. Bagnoud, B. Aurand, A. Blazevic, S. Borneis, C. Bruske, B. Ecker, U. Eisenbarth, J. Fils, A. Frank, E. Gaul *et al.*, Commissioning and early experiments of the PHELIX facility, Appl. Phys. B **100**, 137 (2010).

[53] Z. Zhang, F. Wu, J. Hu, X. Yang, J. Gui, P. Ji, X. Liu, C. Wang, Y. Liu, X. Lu *et al.*, The laser beamline in SULF facility, High Power Laser Sci. Eng. **8**, e4 (2020).

[54] C. Gahn, G. Tsakiris, A. Pukhov, J. Meyer-ter Vehn, G. Pretzler, P. Thirolf, D. Habs, and K. Witte, Multi-MeV electron beam generation by direct laser acceleration in high-density plasma channels, Phys. Rev. Lett. **83**, 4772 (1999).

[55] J. Shaw, N. Lemos, L. D. Amorim, N. Vafaei-Najafabadi, K. Marsh, F. Tsung, W. Mori, and C. Joshi, Role of direct laser acceleration of electrons in a laser wakefield accelerator with ionization injection, Phys. Rev. Lett. **118**, 064801 (2017).

[56] T. Wang, V. Khudik, A. Arefiev, and G. Shvets, Direct laser acceleration of electrons in the plasma bubble by tightly focused laser pulses, Phys. Plasmas **26**, 083101 (2019).

[57] J. Götzfried, A. Döpp, M. Gilljohann, F. Foerster, H. Ding, S. Schindler, G. Schilling, A. Buck, L. Veisz, and

S. Karsch, Physics of high-charge electron beams in laser-plasma wakefields, Phys. Rev. X **10**, 041015 (2020).

[58] O. Rosmej, M. Gyrdymov, M. M. Günther, N. E. Andreev, P. Tavana, P. Neumayer, S. Zähter, N. Zahn, V. S. Popov, N. Borisenko *et al.*, High-current laser-driven beams of relativistic electrons for high energy density research, Plasma Phys. Controlled Fusion **62**, 115024 (2020).

[59] J. D. Jackson, *Classical Electrodynamics*, 3rd ed. (John Wiley & Sons, Inc., NewYork, NY, 1999), p. 5.

[60] B. Kettle, E. Gerstmayr, M. Streeter, F. Albert, R. Baggott, N. Bourgeois, J. Cole, S. Dann, K. Falk, I. Gallardo González *et al.*, Single-shot multi-keV x-ray absorption spectroscopy using an ultrashort laser-wakefield accelerator source, Phys. Rev. Lett. **123**, 254801 (2019).

[61] S. Kneip, S. Nagel, C. Bellei, N. Bourgeois, A. Dangor, A. Gopal, R. Heathcote, S. Mangles, J. Marques, A. Maksimchuk *et al.*, Observation of synchrotron radiation from electrons accelerated in a petawatt-laser-generated plasma cavity, Phys. Rev. Lett. **100**, 105006 (2008).

[62] L. Yi, A. Pukhov, P. Luu-Thanh, and B. Shen, Bright x-ray source from a laser-driven microplasma waveguide, Phys. Rev. Lett. **116**, 115001 (2016).

[63] X. Shen, A. Pukhov, M. Günther, and O. Rosmej, Bright betatron x-rays generation from picosecond laser interactions with long-scale near critical density plasmas, Appl. Phys. Lett. **118**, 134102 (2021).

[64] J. Cikhardt, M. Gyrdymov, S. Zähter, P. Tavana, M. Günther, N. Bukharskii, N. Borisenko, J. Jacoby, X. Shen, A. Pukhov *et al.*, Characterization of bright betatron radiation generated by direct laser acceleration of electrons in plasma of near critical density, Matter Radiat. Extremes **9**, 027201 (2024).

[65] N. Andreev, V. Kirsanov, L. Gorbunov, and A. Sakharov, Linear theory of resonance self-modulation of an intense laser pulse in homogeneous plasma and plasma channels, IEEE Trans. Plasma Sci. **24**, 363 (1996).

[66] O. Vais, M. Lobok, and V. Y. Bychenkov, Compression of high-power laser pulse leads to increase of electron acceleration efficiency, Phys. Rev. E **110**, 065202 (2024).

[67] C. Ren and W. Mori, Physical picture for the laser hosing instability in a plasma, Phys. Plasmas **8**, 3118 (2001).

[68] N. Andreev, V. Kirsanov, and L. Gorbunov, Stimulated processes and self-modulation of a short intense laser pulse in the laser wake-field accelerator, Phys. Plasmas **2**, 2573 (1995).

[69] A. Zhidkov, T. Fujii, and K. Nemoto, Electron self-injection during interaction of tightly focused few-cycle laser pulses with underdense plasma, Phys. Rev. E **78**, 036406 (2008).

[70] S. Fourmaux, S. Corde, K. T. Phuoc, P. Lassonde, G. Lebrun, S. Payeur, F. Martin, S. Sebban, V. Malka, A. Rousse *et al.*, Single shot phase contrast imaging using laser-produced betatron x-ray beams, Opt. Lett. **36**, 2426 (2011).

[71] M. Vranic, O. Klimo, G. Korn, and S. Weber, Multi-GeV electron-positron beam generation from laser-electron scattering, Sci. Rep. **8**, 4702 (2018).